CHAPTER-4

Carbene Driven Stabilization of the H_{red} State of Biomimetic Model [FeFe]-Hydrogenase Complexes.

Abstract: In this chapter, we present our results of theoretical investigation toward stabilization of rotated structure in carbene substituted [FeFe]–hydrogenase model complexes. Stabilization of fully rotated conformation at one of the iron center has been achieved for the reduced Fe(I)Fe(I) state in chelated CAAC substituted biomimetic hydrogenase model complex. This study indicates that the spatial orientation of the chelated NHCs at one of the iron center (Fe_p) plays a major role in determining the geometry at the other (Fe_d). We also made an attempt at explaining the electronic origin behind the favorability of rotated *vs* unrotated structure in asymmetrically substituted chelated *vs* monodentate NHC complexes.

[4.1] Introduction

The non-renewable and hazardous nature of fossil fuels has prompted the scientists to look for alternative sustainable fuels which can fulfill the increasing demand of energy. Dihydrogen (H_2) is one of the possible solutions for this because it is a promising source of energy and can be considered as a "zero-emission" fuel. Therefore, many researchers devoted their studies towards effective production of dihydrogen *via* proton reduction [1]. Nature can do this very efficiently using an enzyme called hydrogenase which can be classified into three main categories as [NiFe], [FeFe] and [Fe]–hydrogenase based on the metal ion composition of their active sites [2,3]. [FeFe]–hydrogenase catalyze the reversible activation of dihydrogen (equation 4.1) involving two key intermediates (H_{ox} and H_{red}, Scheme 4.1) [3c-d,f].

$$H_2 \rightleftharpoons H^- + H^+ \rightleftharpoons 2H^+ + 2e^- \qquad (4.1)$$

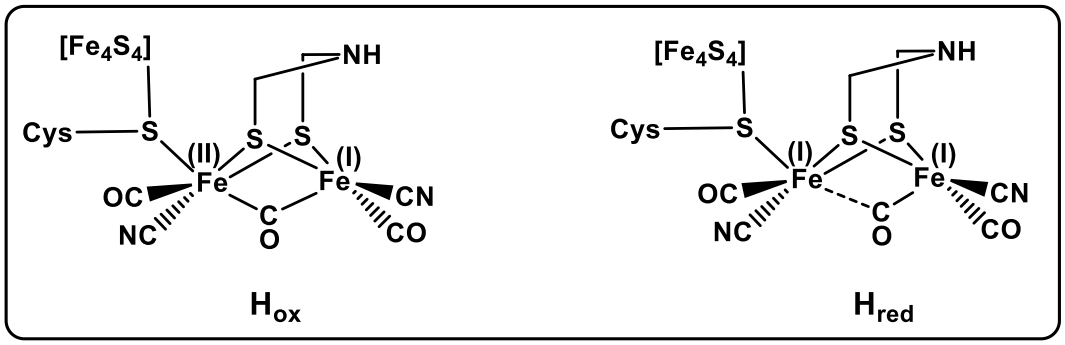

Scheme 4.1: Schematic structures for the active site of [FeFe] – hydrogenase, left: oxidized or mixed valence state (H_{ox}), right: reduced state (H_{red}).

The active site of [FeFe] – H_2ase contains a bimetallic sub cluster [Fe_2S_2] and a [Fe_4S_4] cubane (all together known as H – cluster) linked through a cysteinyl sulphur group [4]. The Fe atoms are referred to as proximal (Fe_p) and distal (Fe_d) with respect to the [Fe_4S_4] cubane and each metal atom contains one CN^- and one CO group. In addition, one CO group bridges the two Fe atoms in the oxidized state (i.e. H_{ox}) [4,5] which transforms to semi-bridging position on one electron reduction (i.e. in H_{red} state) [3e-f,6]. The bimetallic site also contains a cofactor which bridges the two metal centers known as dithiolate cofactor (-SCH_2XCH_2S-). There has been a lot of debate regarding the composition of this cofactor particularly about the nature of the bridgehead atom [7].

However, recent studies provide strong evidence in support of a nitrogen atom i.e., the bridging cofactor is actually an azadithiolate group [8].

Since the structural characterization of the active site of [FeFe]–H_2ase, several experimental and theoretical studies were carried out to mimic the active site of this enzyme with model complexes [1b-d,f,9,10]. While some of them deal with better understanding of the structural features [1b-c,9], others focus on the mechanistic study of the catalytic pathways [1f,10]. One of the important structural features of the H_{ox} and H_{red} state of the native enzyme is the presence of an inverted square pyramidal or fully rotated geometry at Fe_d. The only structural difference between the oxidized (Fe^{II}-Fe^{I}) and reduced (Fe^{I}-Fe^{I}) state is that the carbonyl group between the metal centers is in a semi-bridging position in the H_{red} state, unlike in a completely bridging position in H_{ox} state. The vacant site at Fe_d is the probable site for coordination of H^+/H_2 during reversible dihydrogen production [11]. In 2013, the research groups of Schollhammer [9c] and Rauchfuss [9d] independently reported two model complexes featuring a fully rotated conformation at one of the Fe atom in the reduced Fe^{I}-Fe^{I} state (Scheme 4.2). They reported that the simultaneous presence of three structural features, *viz*, (1) desymmetrization of the two Fe centers, (2) presence of bulky substituent at the dithiolate linkage and most importantly (3) presence of intramolecular agostic interaction between the rotated Fe atom and the dithiolate substituent are necessary to obtain a rotated geometry in the Fe^{I}-Fe^{I} state. In addition, very recently Weigand et al. isolated a sterically stabilized [FeFe]-hydrogenase model complex which exhibits a semi-rotated conformation in Fe^{I}-Fe^{I} state [12].

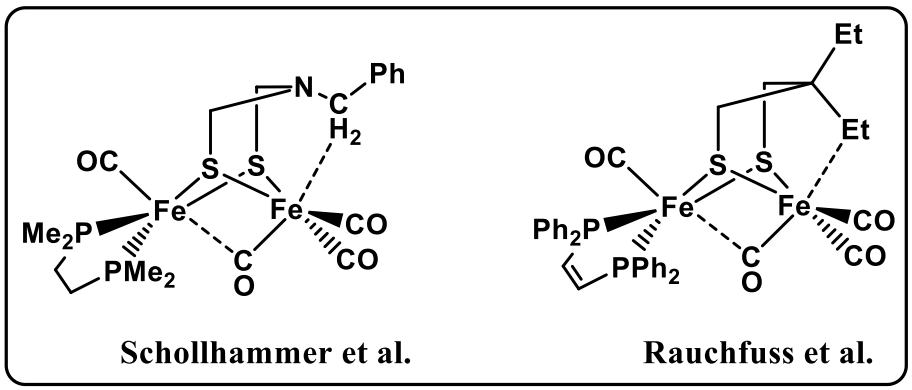

Scheme 4.2: Crystallographically characterized structures for the model complexes with inverted square pyramidal geometry at one of the iron center in the Fe^{I}-Fe^{I} state.

There were reports of *N*-heterocyclic carbenes (NHC) being used as cyanide mimic in the active site models of [FeFe]–H_2ase and few model complexes containing NHCs both in the reduced and oxidized states have been reported [1b-d,9b,13]. Interestingly, Darensbourg et al. discussed the rotated structure of the model complex $\{(\mu\text{-pdt})[Fe(CO)_2PMe_3][Fe(CO)_2IMes]\}^+$ in the mixed valence state which resembles the H_{ox} state of the native enzyme [13]. However, to the best of our knowledge, till date there is no model complex for the [FeFe]–H_2ase active site bearing NHCs as ligand with a rotated structure at one of the Fe center in the reduced Fe^I-Fe^I state. It may be noted that in all these studies, only Arduengo type carbenes were considered while a range of NHCs are known with varying degree of electronic properties [14]. Accordingly, we have investigated the structural features of model complexes with a variety of structurally and electronically different heterocyclic carbenes. In this chapter, we summarize the results obtained from an exploratory study about the possibility of obtaining a rotated structure in the Fe^I-Fe^I state. The model complexes studied were unsymmetrically substituted by both monodentate and chelated NHCs and the bridging cofactor between the two Fe centers is an azadithiolate linkage (Scheme 4.3).

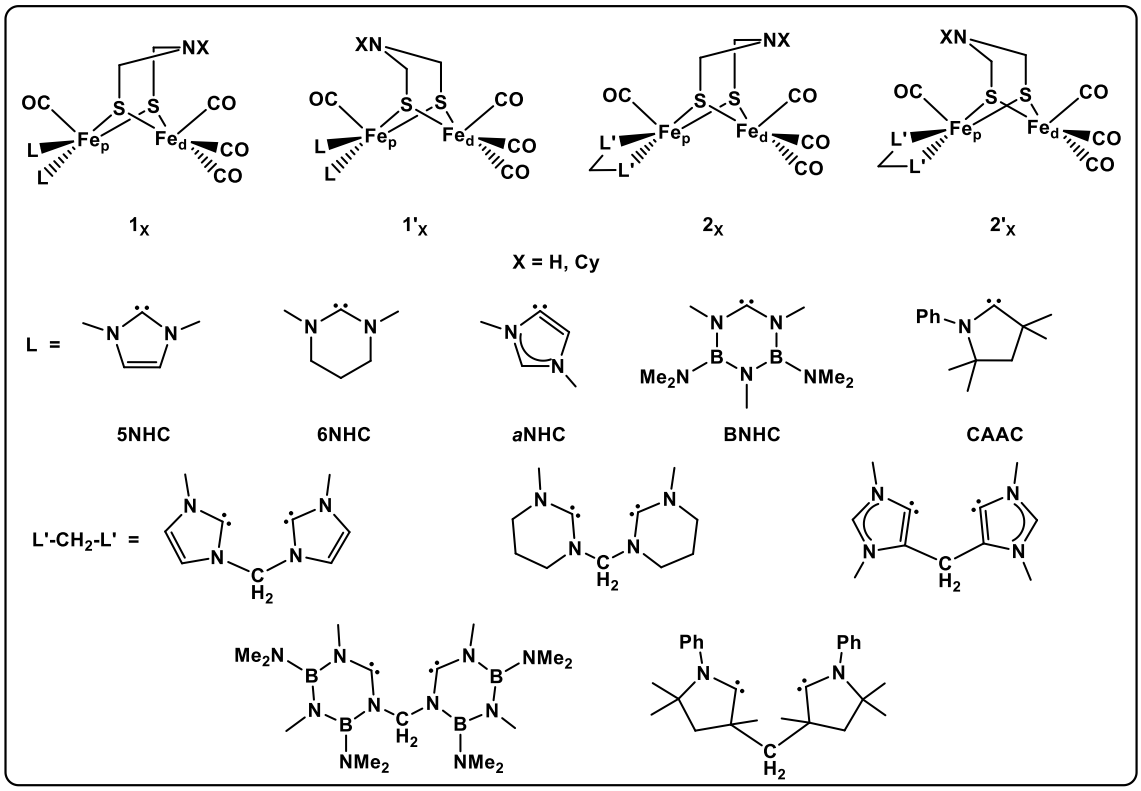

Scheme 4.3: Schematic representation of the molecules considered in the present study (X= H/Cyclohexyl).

Before discussing the methodology and the results, it is necessary to give a description about the nomenclature of the model complexes investigated in this study. The models for the bimetallic active site can be represented by the general formulae (μ-$(SCH_2)_2NX)[Fe(CO)_3][Fe(CO)L_2]$ and (μ-$(SCH_2)_2NX)[Fe(CO)_3][Fe(CO)(L'-CH_2-L')]$ for the monodentate and chelated complexes respectively where X = H/Cyclohexyl and L/L′ = NHCs. As shown in Scheme 4.3, we divided the molecules into two main categories – **1** (with monodentate NHCs) and **2** (with chelated NHCs). The isomers obtained by flipping the azadithiolate linkage are indicated as **1′** and **2′**. The subscript H and Cy is used for X=H and cyclohexyl respectively (*e.g.*, $\mathbf{1_H}$ and $\mathbf{1_{Cy}}$).

[4.2] Computational Details

All the structures were fully optimized in the gas phase without any geometric constraint using BP86 functional [15] incorporated within the Gaussian 03 suit of program [16a]. Even though various studies have reported the validity of this functional in reproducing the structural features of hydrogenase model complexes [9c-d,10e,h,17], we carried out calculations on some representative molecules using hybrid PBE0 [18] as well as meta-GGA M06 [19] exchange-correlation functional. Interestingly, the key geometrical parameters (*e.g.*, Fe_p-Fe_d bond lengths) computed at BP86 level are in better agreement with the experimental values for similar carbene substituted model complexes [1c] compared to those computed using PBE0 and M06 functional (Table 4.1). We have used Def2-TZVP basis set for Fe and Def2-SVP for all other atoms [20]. Calculations using Def2-TZVP basis set for all the atoms with more than 1600 basis functions are much beyond the scope of our available computational resources. However, we indeed performed calculations on few representative molecules using Def2-TZVP basis set for all the atoms and found only marginal differences on the key geometrical parameters as well as on the energy differences between the possible isomers (Tables 4.1 and 4.2). Also, solvent (acetonitrile) and dispersion effects were evaluated for these molecules using polarizable continuum model (PCM) [21] and D3 version of Grimme's dispersion correction coupled with D3 damping function using the keyword "Empirical Dispersion = GD3" as implemented in Gaussian 09 suit of programs [16b]. The nature of the optimized geometries are characterized by calculating their vibrational frequencies at the same level of theory and all of them were found to be minima with real frequencies.

Table 4.1: Calculated values of key geometrical parameters for some representative molecules at different levels of theories.[a]

Complex	Level of Theory	Fe_p-Fe_d	Fe_p-CO_{ap}	C_C-Fe_p-C_C	Fe_d-CO_{bas}
2_H-5NHC	BP86/Def2-SVP, Def2-TZVP (Fe)	2.595	1.746	86.9	1.754 1.754
	BP86/Def2-TZVP	2.601	1.733	86.6	1.754 1.754
	BP86/Def2-TZVP (Including dispersion and solvent)	2.560	1.733	86.2	1.743 1.743
	PBE0/Def2-TZVP	2.549	1.734	86.3	1.744 1.744
	M06/Def2-TZVP	2.557	1.761	86.2	1.761 1.761
$2'_H$-5NHC	BP86/Def2-SVP, Def2-TZVP (Fe)	2.605	1.737	86.9	1.756 1.756
	BP86/Def2-TZVP	2.608	1.727	86.5	1.755 1.755
	BP86/Def2-TZVP (Including dispersion and solvent)	2.569	1.727	85.6	1.743 1.743
	PBE0/Def2-TZVP	2.553	1.727	86.4	1.745 1.745
	M06/Def2-TZVP	2.560	1.752	86.2	1.761 1.761
2_H-CAAC	BP86/Def2-SVP, Def2-TZVP (Fe)	2.603	1.751	93.4	1.753 1.753
	BP86/Def2-TZVP	2.615	1.741	92.9	1.748 1.755
	BP86/Def2-TZVP (Including dispersion and solvent)	2.566	1.743	92.4	1.741 1.741
	PBE0/Def2-TZVP	2.556	1.734	92.6	1.743 1.743
	M06/Def2-TZVP	2.574	1.762	91.8	1.764 1.754
$2'_H$-CAAC	BP86/Def2-SVP, Def2-TZVP (Fe)	2.620	1.741	93.2	1.758 1.750
	BP86/Def2-TZVP	2.648	1.727	92.4	1.760 1.751
	BP86/Def2-TZVP (Including dispersion and solvent)	2.594	1.733	91.4	1.749 1.738
	PBE0/Def2-TZVP	2.572	1.724	92.6	1.749 1.739
	M06/Def2-TZVP	2.581	1.751	91.8	1.764 1.755

[a]The Fe_p-Fe_d bond lengths in experimentally observed complexes falls in the range of 2.577-2.625 Å [1c].

Table 4.2: Calculated zero-point corrected energies of the parent and flipped isomers (in hartree) for some representative molecules and their energy differences (ΔE, in kcal mol^{-1}) at different levels of theories.

Complex	Level of Theory	Parent	Flipped	ΔE
2_H-5NHC vs $2'_H$-5NHC	BP86/Def2-SVP, Def2-TZVP (Fe)	-4479.676432	-4479.672254	2.6
	BP86/Def2-TZVP	-4481.228185	-4481.223902	2.6
	BP86/Def2-TZVP (Including dispersion and solvent)	-4481.336811	-4481.332270	2.8
	PBE0/Def2-TZVP	-4478.536059	-4478.530923	3.2
	M06/Def2-TZVP	-4479.714370	-4479.708179	3.9
2_H-CAAC vs $2'_H$-CAAC	BP86/Def2-SVP, Def2-TZVP (Fe)	-5068.525687	-5068.520636	3.1
	BP86/Def2-TZVP	-5070.690775	-5070.685140	3.5
	BP86/Def2-TZVP (Including dispersion and solvent)	-5070.882787	-5070.877000	3.7
	PBE0/Def2-TZVP	-5067.959366	-5067.952923	4.0
	M06/Def2-TZVP	-5068.739571	-5068.732682	4.3

It should be noted that we have also considered the high spin triplet state for some representative molecules which were found to be in higher energy by 18–28 kcal mol^{-1} (Table 4.3). Further, calculations within conventional unrestricted open-shell singlet as well as broken symmetry (BS) using the spinflip approach were attempted on

Table 4.3: BP86/Def2-SVP, Def2-TZVP(Fe) calculated values of energies (in hartree) for some representative molecules in their respective singlet and triplet spin states as well as the energy difference between singlet and triplet states (ΔE_{S-T}, in kcal mol^{-1}).

Complex	Singlet State Energy	Triplet State Energy	ΔE_{S-T}
1_H-5NHC	-4520.10477	-4520.06721	23.5
2_H-5NHC	-4479.67643	-4479.63348	26.9
2_H-6NHC	-4560.518484	-4560.486197	20.2
2_H-aNHC	-4558.154585	-4558.109419	28.3
2_H-CAAC	-5068.525687	-5068.496805	18.1
2_H-BNHC	-5151.350086	-5151.318442	19.8

symmetrically substituted related model systems. However, calculations show that frontier orbitals are not 'purely' centred on the Fe atoms, that is, the spin-state of the

compounds are not dictated by the electrons within the metal centers nor by magnetic interactions between these centers. Such a situation is in line with the results reported in this work furthermore validating the use of spin-restricted calculations constraining the total electronic spin along a reference axis to zero.

[4.3] Results and Discussion

Unsymmetrical substitution of the diiron center for the Fe(I)Fe(I) state is carried out using both monodentate and chelated NHCs. In all of these complexes, we have considered only the basal/basal isomer with respect to NHC coordination at Fe as X-ray diffraction study confirms that the bis-carbene ligand is in a basal/basal environment in similar experimentally known complexes [1c]. Further, the recent synthesis of diiron compounds modeling the H_{red} state has the electron donor phosphorus arms at the basal positions [9c,d]. The carbene substituted Fe center is referred as proximal (Fe_p) whereas the other one as distal (Fe_d) (Scheme 4.3). It should be noted that geometry optimization of all the model complexes were carried out starting from an unrotated (i.e., all terminal) geometry.

[4.3.1] Model Complexes with Normal Five-Membered NHCs (5NHC)

As mentioned above, we have considered both monodentate and chelated 5NHCs as the substituents for the proximal iron center (Fe_p). However, we did not get rotated structures for monodentate 5NHCs as substituents at Fe_p even though the $Fe_d(CO)_3$ unit is distorted to some extent (C_{CO}-Fe_p-Fe_d-C_{CO} dihedral angle is 16.2° and 7.7° for **1_H-5NHC** and **$1'_H$-5NHC** respectively, where C_{CO} stands for carbonyl carbon). The distortion is somewhat greater for complexes with bulky substituent (i.e. cyclohexyl) in the azadithiolate group. In case of the chelated complexes, we have installed the 5NHC ligands at Fe_p in a similar fashion (Scheme 4.4(a)) to that in the experimentally known model complex [(μ-pdt)[Fe(*Che*-5NHC)$(CO)_4$] [1c] (*Che* = chelated) having an unrotated geometry. As expected, optimization of all the chelated complexes (**2_X-5NHC** and **$2'_X$-5NHC**) lead to unrotated structures. It should be noted that in all these complexes, the NHC rings are positioned below the Fe_p–Fe_d vector (Scheme 4.4 (a)) and this may be the reason for not obtaining a rotated conformation as this particular orientation of the chelated NHCs sterically prevent the movement of one of the basal CO

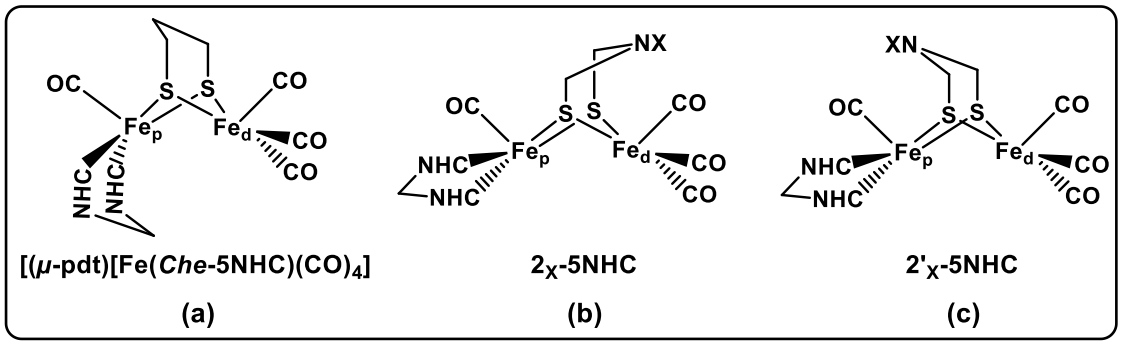

Scheme 4.4: Schematic representations of the difference in orientation of the chelated 5NHC ligands in (a) **[(*μ*-pdt)[Fe(*Che*-5NHC)(CO)$_4$]**, (b) **2**x**-5NHC** and (c) **2'**x**-5NHC**, where X= H/Cy.

unit at the distal iron center to a bridging position between the iron centers. Therefore, we envisage that it may be possible to get the rotated conformation for these complexes by considering a different orientation of the chelated 5NHCs around Fe_p. Accordingly, we have optimized all the chelated complexes starting from a geometry where the NHC rings are moved away from the proximal iron center (Scheme 4.4 (b) and 4.4 (c)) thus making room for transfer of a CO group at Fe_d to occupy a bridging position between Fe_p and Fe_d centres. Interestingly, complete rotation of the $Fe_d(CO)_3$ unit is observed with this particular orientation of chelated 5NHCs around Fe_p thereby resulting in an inverted square pyramidal geometry at Fe_d with a semi-bridging carbonyl group between the two iron centers (Figure 4.1) implying that the orientation of the chelated NHC ligands at Fe_p plays a crucial role in determining the geometry at Fe_d. Coordination of the chelated NHCs forms a six- membered metallacycle at Fe_p (Fe_p-C_C-N-C-N-C_C ring, C_C stands for carbene carbon) which adopts a boat like conformation (Figure 4.2). The calculated values of Addison τ parameter [22] for the rotated structures are found to be close to zero

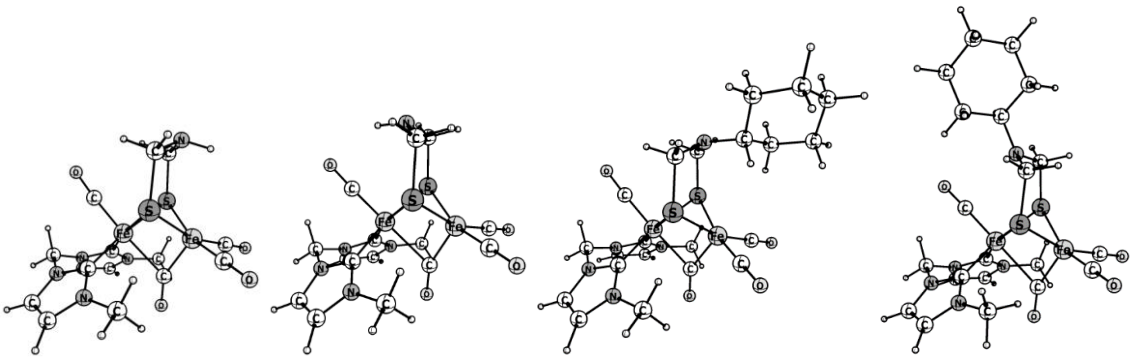

Figure 4.1: Optimized rotated structures for the model complexes with chelated 5NHCs.

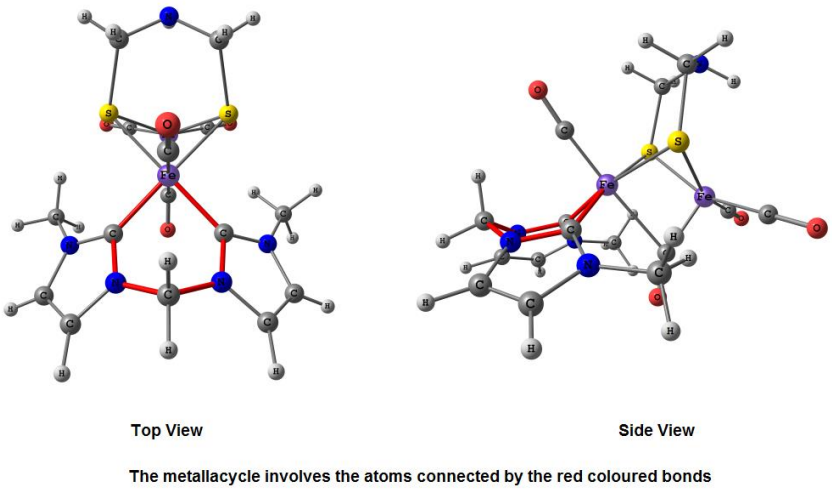

Figure 4.2: Figure showing the metallacycle formed at Fe_p as a result of coordination of the chelated 5NHC rings in complex **2_H-5NHC**.

which is in accordance with a perfectly inverted square-pyramidal, i.e., fully-rotated geometry at Fe_d. In addition, the C_{CO}-Fe_p-Fe_d-C_{CO} dihedral angle is also found to be significantly large (107.3°). It is observed that the chelated complexes with rotated geometries have substantially shorter Fe_p-Fe_d bond lengths (2.595-2.605Å) compared to those with monodentate ones (i.e., **1_X-5NHC** and **$1'_X$-5NHC**, 2.715-2.741Å). Chelation results in not only symmetric coordination of the NHC ligands with equal Fe_p–C_C bond lengths but also greater degree of stabilization of the Fe_p–Fe_d bonding interaction in the rotated geometry. An MO analysis for both **1_H-5NHC** and **2_H-5NHC** (Figure 4.3) shows that in **1_H-5NHC**, the MO representing the Fe_p-Fe_d bonding interaction is HOMO−1 (−4.1 eV) while in **2_H-5NHC**, the same turned out to be significantly stable and becomes HOMO−8 (−5.6 eV).

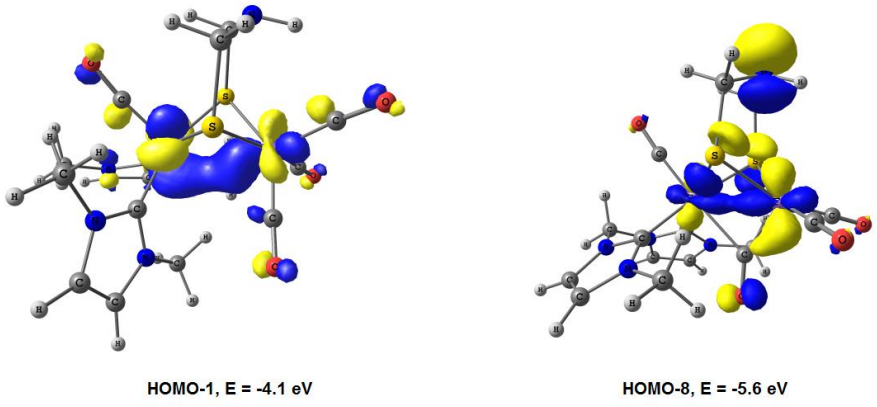

Figure 4.3: Molecular orbital representing the Fe_p–Fe_d bonding interaction in (a) **1_H-5NHC** and (b) **2_H-5NHC**.

It should be noted that the rotated structure of the flipped isomer **2′$_H$-5NHC** is found to lie in higher energy (by 2.6 kcal mol^{-1}) than that of the parent one (**2$_H$-5NHC**) thereby indicating that the non-bonded interaction (between Fe_d·····HN) gives an additional stabilization to the rotated geometry which is in accordance with previous studies [9c-d,12]. Inclusion of solvent and dispersion in the computational model found to have marginal effect on the energy difference (ΔE = 2.8 kcal mol^{-1}) between the parent and flipped isomer. The ΔE value increases to 3.2 kcal mol^{-1} at the PBE0/Def2-TZVP level of theory and further increases to 3.9 kcal mol^{-1} on being computed using the meta-GGA M06 functional. Similar is the case for complexes with bulky azadithiolate substituent where the un-flipped isomer (**2$_{Cy}$-5NHC**) is found to be 4.8 kcal mol^{-1} more stable than the flipped isomer (**2′$_{Cy}$-5NHC**). Interestingly, the calculated ν_{CO} values for **2$_{Cy}$-5NHC** are very close to the theoretically assigned values for the recently reported biomimetic complex having a rotated geometry [9d].

However, the rotated isomers in case of **2$_X$-5NHC** and **2′$_X$-5NHC** complexes are found to be unstable than the unrotated ones (by 5.6 − 11.4 kcal mol^{-1}, Table 4.4) which explains why [(μ-pdt)[Fe(*Che*-5NHC)(CO)$_4$] gets crystalized in an unrotated form despite the presence of chelated 5NHCs. It should be noted that the rotated structure is observed (although higher in energy) only with chelated 5NHCs and accordingly, we have considered only the chelated versions of the remaining four different types of NHCs (Scheme 4.3) as substituents at the proximal iron center.

Table 4.4: BP86/Def2-SVP, Def2-TZVP(Fe) calculated zero point corrected energies (in hartree) of the rotated and unrotated isomers with chelated 5NHCs as well as their energy differences ($\Delta E_{rot\text{-}unrot}$, in kcal mol^{-1}). Negative sign indicates unrotated isomer is more stable.

Complex	Rotated	Unrotated	$\Delta E_{rot\text{-}unrot}$
2$_H$-5NHC	−4479.676432	−4479.689194	−8.0
2'$_H$-5NHC	−4479.672254	−4479.690042	−11.1
2$_{Cy}$-5NHC	−4714.019999	−4714.028929	−5.6
2'$_{Cy}$-5NHC	−4714.012236	−4714.030470	−11.4

[4.3.2] Model Complexes with Normal Six-Membered NHCs (6NHC), Abnormal NHCs (*a*NHC) and Boron Substituted NHCs (BNHC)

Optimizations were carried out using the chelated versions of all these three types of NHCs (Scheme 4.3) by considering the different *Che*-NHC orientations around Fe_p as shown in Scheme 4.4. Interestingly, here also, complete rotation of the $Fe_d(CO)_3$ unit is observed when the chelated NHCs orients away from the proximal iron center as shown in Scheme 4.4(b) and 4.4(c). However, unfortunately all these three types of NHCs also fail to stabilize the rotated conformer as compared to the unrotated ones (Table 4.5). It may be noted that the energy difference between the rotated and unrotated isomers of **2_{Cy}-*a*NHC** is comparatively lower (4.2 kcal mol^{-1}) as compared to all the other complexes and the computed average ν_{CO} value for **$2'_{Cy}$-*a*NHC** (1921 cm^{-1}) is very close to the average ν_{CO} value obtained for the reduced form of the enzyme *Desulfovibrio desulfuricans* (average 1925 cm^{-1}) [5b].

Table 4.5: BP86/Def2-SVP, Def2-TZVP(Fe) calculated zero point corrected energies (in hartree) of the rotated and unrotated isomers of **2_X-6NHC**, **$2'_X$-6NHC**, **2_X-*a*NHC**, **$2'_X$-*a*NHC**, **2_X-BNHC** and **$2'_X$-BNHC** complexes as well as their energy differences ($\Delta E_{rot-unrot}$, in kcal mol^{-1}). Negative sign indicates unrotated isomer is more stable.

Complex	Rotated	Unrotated	$\Delta E_{rot-unrot}$
2_H-6NHC	−4560.518484	−4560.540771	−13.9
$2'_H$-6NHC	−4560.512826	−4560.541364	−17.9
2_{Cy}-6NHC	−4794.863155	−4794.879843	−10.5
$2'_{Cy}$-6NHC	−4794.852028	−4794.881382	−18.4
2_H-*a*NHC	−4558.154585	−4558.167177	−7.9
$2'_H$-*a*NHC	−4558.151212	−4558.168326	−10.7
2_{Cy}-*a*NHC	−4792.499342	−4792.506189	−4.2
$2'_{Cy}$-*a*NHC	−4792.489852	−4792.508949	−11.9
2_H-BNHC	−5151.350086	−5151.370903	−13.0
$2'_H$-BNHC	−5151.344584	−5151.372043	−17.2
2_{Cy}-BNHC	−5385.694949	−5385.710405	−9.7
$2'_{Cy}$-BNHC	−5385.683894	−5385.710609	−16.7

[4.3.3] Model Complexes with Cyclic Alkyl Amino Carbene (CAAC)

Recent advances in carbene chemistry shows that cyclic(alkyl)(amino)carbene (CAAC) possesses better ligand properties than classical NHCs in terms of both electron donation and acceptance ability [14a-c,23]. Therefore, we have considered CAAC as one of the possible substituent at the proximal iron site and the chelation of the two CAAC ligands were carried out through the sp^3 hybridized carbon atoms (Scheme 4.3). Optimizations of all the chelated CAAC substituted complexes starting from a geometry where the orientation of the chelated CAAC ligands is similar to that in the experimentally isolated one (Scheme 4.4(a)) lead to unrotated structures with all terminal CO groups at Fe_d. Further, incorporation of chelated CAAC groups at Fe_p in a similar fashion as shown in Scheme 4.4(b) and 4.4(c) leads to rotation of the $Fe_d(CO)_3$ unit and results in a perfectly inverted square pyramidal geometry which is confirmed by the calculated values of Addison τ parameter (~ 0.0). However, as compared to the previous complexes with all the variants of NHCs, the energy difference between the rotated and unrotated isomers for the complexes **2_H-CAAC** and **2_{Cy}-CAAC** are minimal (Table 4.6). In fact, the rotated isomer of **2_{Cy}-CAAC** is found to be slightly more stable (by 0.45 kcal mol^{-1}) than the unrotated one which increases to 5.4 kcal mol^{-1} as a result of inclusion of dispersion in the computational model. To confirm it further, we have performed additional calculations using the dispersion corrected WB97XD and the meta-GGA M06 functional and both these functional too indicate the higher stability (by 4.0 kcal mol^{-1}) of the rotated isomer of **2_{Cy}-CAAC**. Further, the computed $Fe_d\cdots H_{Cy}$ bond distance in the rotated isomer of **2_{Cy}-CAAC** (2.781 Å) is in close agreement with experimentally reported model complex for the H_{red} state with a rotated geometry (Fe·····HC = 2.750 Å)

Table 4.6: BP86/Def2-SVP, Def2-TZVP(Fe) calculated zero point corrected energies (in hartree) of the rotated and unrotated isomers with chelated CAACs as well as their energy differences ($\Delta E_{rot\text{-}unrot}$, in kcal mol^{-1}). Negative sign indicates unrotated isomer is more stable.

Complex	Rotated	Unrotated	$\Delta E_{rot\text{-}unrot}$
2_H-CAAC	−5068.525683	−5068.528589	−1.8
$2'_H$-CAAC	−5068.520636	−5068.530885	−6.4
2_{Cy}-CAAC	−5302.871013	−5302.870326	0.4
$2'_{Cy}$-CAAC	−5302.859441	−5302.871056	−7.2

[9c]. All these observations for the rotated isomer of **2_{Cy}-CAAC** is in accordance with previous experimental and theoretical studies which states that the simultaneous presence of three structural features, *viz*, (1) desymmetrization of the two Fe centers, (2) presence of bulky substituent at the dithiolate linkage and most importantly (3) presence of intramolecular agostic interaction between the rotated Fe atom and the dithiolate substituent are necessary to obtain a completely inverted or fully rotated geometry in the Fe^{I}-Fe^{I} state. Further, the energy difference between the rotated and the more stable unrotated isomers of **2_{H}-CAAC** is only 1.8 kcal mol^{-1} thereby indicating that depending on the experimental conditions, one isomer may be preferred over the other. Interestingly, the average ν_{CO} value for **2_{H}-CAAC** (1925 cm^{-1}) is in excellent agreement with that obtained for the reduced form of the enzyme *Desulfovibrio desulfuricans* [5b]. Further, **2_{Cy}-CAAC** also possesses average ν_{CO} values (1918 cm^{-1}) which is very close to that observed for enzyme active site.

[4.3.4] To Rotate or not to Rotate? The Role of Chelation

It should be noted that all the optimizations were carried out starting from an unrotated or all terminal geometry considering a variety of NHCs and we observe complete rotation of the $Fe_d(CO)_3$ unit only for the complexes with chelated NHC ligands but not with the monodentate ones. Further, the rotation of the $Fe_d(CO)_3$ unit is observed only for a particular orientation of the chelated NHCs. As stated earlier, the spatial orientation of the chelated NHCs as shown in Scheme 4.4(a) sterically prevents the movement of one of the basal CO unit at the distal iron center to a bridging position between the iron centers. However, in the other cases i.e., as shown in Scheme 4.4(b) and 4.4(c), the NHC rings are moved away from the proximal iron center thus making room for transfer of a CO group at Fe_d to occupy a bridging position between Fe_p and Fe_d centres resulting in a rotated structure at Fe_d. However, still the question is "why rotation of the distal iron core is observed only with chelated NHCs but not with monodentate ones (even though the rotated structure is higher in energy than the unrotated one)?". Accordingly, to unravel the role of chelation toward obtaining the rotated geometry, we have performed an in depth molecular orbital analysis for **1_{H}-CAAC** and **2_{H}-CAAC** and the results are discussed below.

The rotation of $Fe_d(CO)_3$ unit in the chelated complexes is a consequence of significant increase in electron density at the proximal iron center. In case of the

monodentate complexes, there is a minor difference in the interaction of one of the CAAC ligands with the proximal iron center compared to the other which may be attributed to the difference in spatial orientation of both the CAACs. However, the restricted rotation of the CAAC ligands upon chelation results in stronger overlap between the carbene lone pair orbitals and vacant d-orbital of the iron center which is further corroborated by the calculated shorter Fe_p-C_C bond lengths for the chelated complex (1.970/1.970 Å) compared to those with monodentate ones (1.980/1.990 Å). A closer look at Figure 4.4 shows that in **1_H-CAAC**, the lone pair orbital of one of the CAAC ligands weakly overlap with the vacant metal d-orbital while both the donor sites interact equally in **2_H-CAAC** thereby forming two equal Fe_p-C_C bonds. Further, the increase in electron density at the proximal iron center upon chelation of the CAACs (i.e., in **2_H-CAAC**) is also evident from an increase in the values of natural charge (−0.284) and natural valence population (8.222) at Fe_p compared to those in **1_H-CAAC** (−0.117 and 8.064 respectively). The electron rich proximal iron center undergoes electronic relaxation by transferring some of the excess electron density to the π*−orbital of one of the basal CO group at Fe_d thereby bringing this CO group to a semi-bridging position (Figure 4.5). The stepwise changes in Fe_p-Fe_d bonding interaction as well as the formation of new Fe_p-CO_{bridg} bond during inversion of the $Fe_d(CO)_3$ unit for **2_H-CAAC** is shown in Figure 4.6.

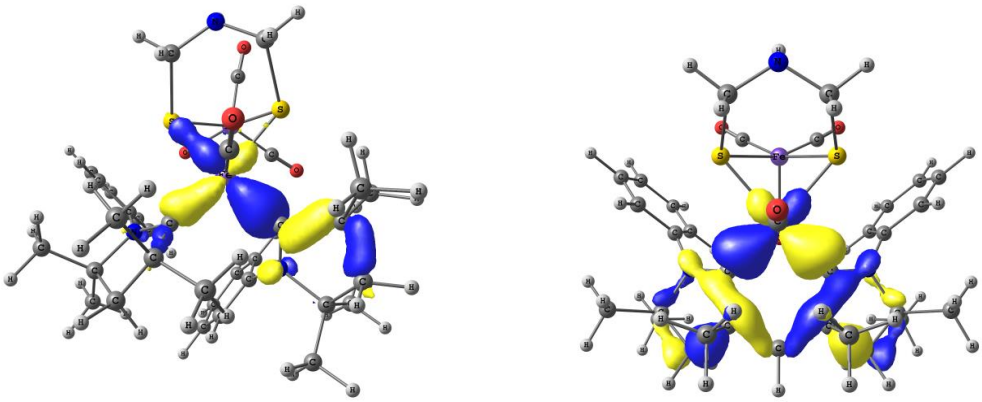

(a) (b)

Figure 4.4: Molecular orbital representing the overlap between the lone pairs of CAAC and metal d-orbitals in (a) **1_H-CAAC** and (b) **2_H-CAAC**.

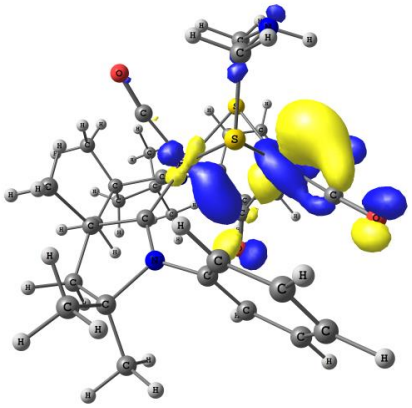

Figure 4.5: Molecular orbital showing the interaction between the proximal iron center (Fe_p) and bridging carbonyl group in **2_H-CAAC**.

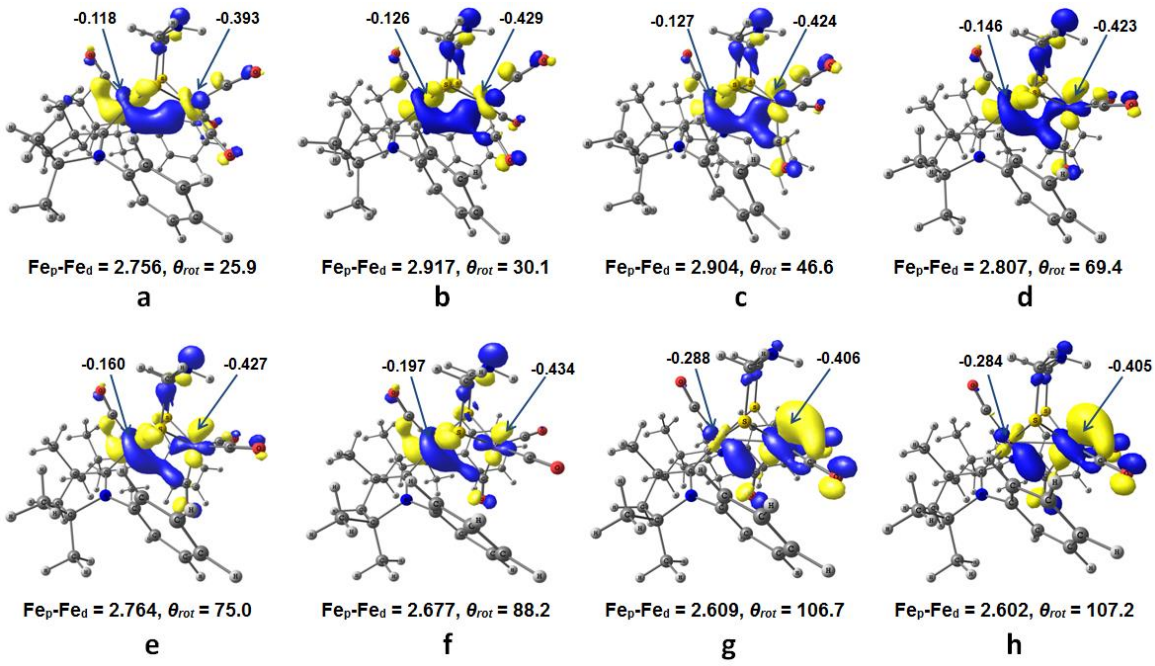

Figure 4.6: Molecular orbitals representing the stepwise change of Fe_p-Fe_d bonding interaction as well as formation of new Fe_p-CO_{bridg} bond during rotation of $Fe_d(CO)_3$ unit in **2_H-CAAC**. The values represented by the arrows are natural charges at Fe_p (left) and Fe_d (right). θ_{rot} ($\angle C_{CO}$-Fe_p-Fe_d-C_{CO}) represents the dihedral angle reflecting rotation at $Fe_d(CO)_3$ unit (C_{CO} represents carbon atom of the carbonyl group). The values of Fe_p-Fe_d bond lengths and θ_{rot} are given in Å and degrees respectively.

[4.4] Conclusions

This theoretical study reveals that chelation of the carbenes at the proximal iron center may lead to a fully rotated structure for the [FeFe]-hydrogenase model complexes. However, the spatial orientation of the chelated carbenes at the proximal iron center plays a major role in determining the geometry at the distal iron center. Interestingly, the CAAC anchored complexes such as **2_H-CAAC** and **2_{Cy}-CAAC** are found to be suitable candidate towards obtaining a rotated structure and invite experimental verification. In addition, the higher stability of the rotated isomer of **2_{Cy}-CAAC** as compared to the unrotated one is in accordance with the previous experimental observation of fully rotated structure in asymmetrically substituted complex with a bulky substituent at the dithiolate bridgehead. In view of the paucity of biomimetic model complexes with a rotated structure for the H_{red} state of [FeFe]-hydrogenase, we hope that our study will inspire experimental chemists towards designing of model systems with a rotated structure.

[4.5] Bibliography

[1] (a) Nehring, J. L. and Heinekey, D. M. Dinuclear Iron Isonitrile Complexes: Models for the Iron Hydrogenase Active Site. *Inorganic Chemistry*, 42(14):4288-4292, 2003. (b) Capon, J. F., Hassnaoui, S. E., Gloaguen, F., Schollhammer, P., and Talarmin, J. N-Heterocyclic Carbene Ligands as Cyanide Mimics in Diiron Models of the All-Iron Hydrogenase Active Site. *Organometallics*, 24(9):2020-2022, 2005. (c) Morvan, D., Capon, J. F., Gloaguen, F., Le Goff, A., Marchivie, M., Michaud, F., Schollhammer, P., Talarmin, J., and Yaouanc, J. J. N-Heterocyclic Carbene Ligands in Nonsymmetric Diiron Models of Hydrogenase Active Sites. *Organometallics*, 26(8):2042-2052, 2007. (d) Morvan, D., Capon, J. F., Gloaguen, F., Pétillon, F. Y., Schollhammer, P., Talarmin, J., and Kervarec, N. Modeling [FeFe] Hydrogenase: Synthesis and Protonation of a Diiron Dithiolate Complex Containing a Phosphine-N-Heterocyclic-Carbene Ligand. *Journal of Organometallic Chemistry*, 694(17):2801-2807, 2009. (e) Harb, M. K., Apfel, U. P., Sakamoto, T., El-khateeb, M., and Weigand, W. Diiron Dichalcogenolato (Se and Te) Complexes: Models for the Active Site of [FeFe] Hydrogenase. *European Journal of Inorganic Chemistry*, 2011(7):986-993, 2011. (f) Carroll, M. E., Barton, B. E., Rauchfuss, T. B., and Carroll, P. J. Synthetic Models for the Active Site of the [FeFe]-Hydrogenase: Catalytic Proton Reduction and the Structure of the Doubly Protonated Intermediate. *Journal of the American Chemical Society*, 134(45):18843-18852, 2012. (g) Bourrez, M., Steinmetz, R., and Gloaguen, F. Mechanistic Insights into the Catalysis of Electrochemical Proton Reduction by a Diiron Azadithiolate Complex. *Inorganic Chemistry*, 53(19):10667-10673, 2014. (h) Gloaguen, F. Electrochemistry of Simple Organometallic Models of Iron–Iron Hydrogenases in Organic Solvent and Water. *Inorganic Chemistry*, 55(2):390-398, 2016.

[2] (a) Adams, M. W. The Structure and Mechanism of Iron-Hydrogenases. *Biochimica et Biophysica Acta (BBA)-Bioenergetics*, 1020(2):115-145, 1990. (b) Garcin, E., Vernede, X., Hatchikian, E. C., Volbeda, A., Frey, M., and Fontecilla-Camps, J. C. The Crystal Structure of a Reduced [NiFeSe] Hydrogenase Provides an Image of the Activated Catalytic Center. *Structure*, 7(5):557-566, 1999. (c) Korbas, M., Vogt, S., Meyer-Klaucke, W., Bill, E., Lyon, E. J., Thauer, R. K., and Shima, S. The Iron-Sulfur Cluster-Free Hydrogenase (Hmd) is a Metalloenzyme with a Novel Iron Binding Motif. *Journal of Biological Chemistry*, 281(41):30804-30813, 2006.

[3] (a) Siegbahn, P. E., Tye, J. W., and Hall, M. B. Computational Studies of [NiFe] and [FeFe] Hydrogenases. *Chemical Reviews*, 107(10):4414-4435, 2007. (b) Lubitz, W., Reijerse, E., and Gastel, M. v. [NiFe] and [FeFe] Hydrogenases Studied by Advanced Magnetic Resonance Techniques. *Chemical Reviews*, 107(10):4331-4365, 2007. (c) Fontecilla-Camps, J. C., Volbeda, A., Cavazza, C., and Nicolet, Y. Structure/Function Relationships of [NiFe]-and [FeFe]-Hydrogenases. *Chemical Reviews*, 107(11):4273−4303, 2007. (d) Tard, C. and Pickett, C. J. Structural and Functional Analogues of the Active Sites of the [Fe]-,[NiFe]-, and [FeFe]-Hydrogenases. *Chemical Reviews*, 109(6):2245-2274, 2009. (e) Lubitz, W., Ogata, H., Rüdiger, O., and Reijerse, E. Hydrogenases. *Chemical Reviews*, 114(8):4081-4148, 2014. (f) Simmons, T. R., Berggren, G., Bacchi, M., Fontecave, M., and Artero, V. Mimicking Hydrogenases: From Biomimetics to Artificial Enzymes. *Coordination Chemistry Reviews*, 270:127-150, 2014.

[4] (a) Peters, J. W., Lanzilotta, W. N., Lemon, B. J., and Seefeldt, L. C. X-ray Crystal Structure of the Fe-Only Hydrogenase (CpI) from Clostridium Pasteurianum to 1.8 Angstrom Resolution. *Science*, 282(5395):1853-1858, 1998. (b) Nicolet, Y., Piras, C., Legrand, P., Hatchikian, C. E., and Fontecilla-Camps, J. C. Desulfovibrio Desulfuricans Iron Hydrogenase: The Structure Shows Unusual Coordination to an Active Site Fe Binuclear Center. *Structure*, 7(1):13-23, 1999.

[5] (a) Chen, Z., Lemon, B. J., Huang, S., Swartz, D. J., Peters, J. W., and Bagley, K. A. Infrared Studies of the CO-Inhibited Form of the Fe-Only Hydrogenase from Clostridium Pasteurianum I: Examination of its Light Sensitivity at Cryogenic Temperatures. *Biochemistry*, 41(6):2036-2043, 2002. (b) Roseboom, W., De Lacey, A. L., Fernandez, V. M., Hatchikian, E. C., and Albracht, S. P. The Active Site of the [FeFe]-Hydrogenase from Desulfovibrio Desulfuricans. II. Redox Properties, Light Sensitivity and CO-Ligand Exchange as Observed by Infrared Spectroscopy. *Journal of Biological Inorganic Chemistry*, 11(1):102-118, 2006.

[6] Nicolet, Y., De Lacey, A. L., Vernède, X., Fernandez, V. M., Hatchikian, E. C., and Fontecilla-Camps, J. C. Crystallographic and FTIR Spectroscopic Evidence of Changes in Fe Coordination Upon Reduction of the Active Site of the Fe-Only Hydrogenase from Desulfovibrio Desulfuricans. *Journal of the American Chemical Society*, 123(8):1596-1601, 2001.

[7] (a) Foerster, S., Gastel, M. v., Brecht, M., and Lubitz, W. An Orientation-Selected ENDOR and HYSCORE Study of the Ni-C Active State of Desulfovibrio Vulgaris Miyazaki F Hydrogenase. *Journal of Biological Inorganic Chemistry*, 10(1):51-62, 2005. (b) Brecht, M., Gastel, M. v., Buhrke, T., Friedrich, B., and Lubitz, W. Direct Detection of a Hydrogen Ligand in the [NiFe] Center of the Regulatory H_2-Sensing Hydrogenase from Ralstonia Eutropha in Its Reduced State by HYSCORE and ENDOR Spectroscopy. *Journal of the American Chemical Society*, 125(43):13075-13083, 2003. (c) Pandey, A. S., Harris, T. V., Giles, L. J., Peters, J. W., and Szilagyi, R. K. Dithiomethylether as a Ligand in the Hydrogenase H-Cluster. *Journal of the American Chemical Society*, 130(13):4533-4540, 2008.

[8] (a) Schilter, D. and Rauchfuss, T. B. And the Winner is Azadithiolate: An Amine Proton Relay in the [FeFe] Hydrogenases. *Angewandte Chemie International Edition*, 52(51):13518-13520, 2013. (b) Adamska-Venkatesh, A., Roy, S., Siebel, J. F., Simmons, T. R., Fontecave, M., Artero, V., and Lubitz, W. Spectroscopic Characterization of the Bridging Amine in the Active Site of [FeFe] Hydrogenase Using Isotopologues of the H-Cluster. *Journal of the American Chemical Society*, 137(40):12744-12747, 2015. (c) Berggren, G., Adamska, A., Lambertz, C., Simmons, T. R., Esselborn, J., Atta, M., Gambarelli, S., Mouesca, J. M., Reijerse, E., Lubitz, W., and Happe, T. Biomimetic Assembly and Activation of [FeFe]-Hydrogenases. *Nature*, 499(7456):66-69, 2013. (d) Esselborn, J., Lambertz, C., Adamska-Venkatesh, A., Simmons, T., Berggren, G., Noth, J., Siebel, J., Hemschemeier, A., Artero, V., Reijerse, E., and Fontecave, M. Spontaneous Activation of [FeFe]-Hydrogenases by an Inorganic [2Fe] Active Site Mimic. *Nature Chemical Biology*, 9(10):607-609, 2013.

[9] (a) Bruschi, M., Fantucci, P., and De Gioia, L. Density Functional Theory Investigation of the Active Site of Fe-Hydrogenases. Systematic Study of the Effects of Redox State and Ligands Hardness on Structural and Electronic Properties of Complexes Related to the $[2Fe]_H$ Subcluster. *Inorganic Chemistry*, 43(12):3733-3741, 2004. (b) Tye, J. W., Lee, J., Wang, H. W., Mejia-Rodriguez, R., Reibenspies, J. H., Hall, M. B., and Darensbourg, M. Y. Dual Electron Uptake by Simultaneous Iron and Ligand Reduction in an N-Heterocyclic Carbene Substituted [FeFe] Hydrogenase Model Compound. *Inorganic Chemistry*, 44(16):5550-5552, 2005. (c) Munery, S., Capon, J. F., De Gioia, L., Elleouet, C., Greco, C., Pétillon, F. Y., Schollhammer, P., Talarmin, J., and Zampella,

G. New Fe^{I}–Fe^{I} Complex Featuring a Rotated Conformation Related to the $[2Fe]_{H}$ Subsite of [Fe–Fe] Hydrogenase. *Chemistry-A European Journal*, 19(46):15458-15461, 2013. (d) Wang, W., Rauchfuss, T. B., Moore, C. E., Rheingold, A. L., De Gioia, L., and Zampella, G. Crystallographic Characterization of a Fully Rotated, Basic Diiron Dithiolate: Model for the H_{red} State. *Chemistry-A European Journal*, 19(46):15476-15479, 2013.

[10] (a) Olsen, M. T., Barton, B. E., and Rauchfuss, T. B. Hydrogen Activation by Biomimetic Diiron Dithiolates. *Inorganic Chemistry*, 48(16):7507-7509, 2009. (b) Liu, C., Peck, J. N., Wright, J. A., Pickett, C. J., and Hall, M. B. Density Functional Calculations on Protonation of the [FeFe]-Hydrogenase Model Complex $Fe_2(\mu\text{-pdt})(CO)_4(PMe_3)_2$ and Subsequent Isomerization Pathways. *European Journal of Inorganic Chemistry*, 2011(7):1080-1093, 2011. (c) Camara, J. M. and Rauchfuss, T. B. Combining Acid–Base, Redox and Substrate Binding Functionalities to Give a Complete Model for the [FeFe]-Hydrogenase. *Nature Chemistry*, 4(1):26-30, 2012. (d) Wang, Y. and Ahlquist, M. S. Mechanistic Studies on Proton Transfer in a [FeFe] Hydrogenase Mimic Complex. *Dalton Transactions*, 42(21):7816-7822, 2013. (e) Greco, C. H_2 Binding and Splitting on a New-Generation [FeFe]-Hydrogenase Model Featuring a Redox-Active Decamethylferrocenyl Phosphine Ligand: A Theoretical Investigation. *Inorganic Chemistry*, 52(4):1901-1908, 2013. (f) Bourrez, M., Steinmetz, R., and Gloaguen, F. Mechanistic Insights into the Catalysis of Electrochemical Proton Reduction by a Diiron Azadithiolate Complex. *Inorganic Chemistry*, 53(19):10667-10673, 2014. (g) Wang, W., Rauchfuss, T. B., Zhu, L., and Zampella, G. New Reactions of Terminal Hydrides on a Diiron Dithiolate. *Journal of the American Chemical Society*, 136(15):5773-5782, 2014. (h) Huynh, M. T., Wang, W., Rauchfuss, T. B., and Hammes-Schiffer, S. Computational Investigation of [FeFe]-Hydrogenase Models: Characterization of Singly and Doubly Protonated Intermediates and Mechanistic Insights. *Inorganic Chemistry*, 53(19):10301-10311, 2014.

[11] De Lacey, A. L., Fernández, V. M., Rousset, M., and Cammack, R. Activation and Inactivation of Hydrogenase Function and the Catalytic Cycle: Spectroelectrochemical Studies. *Chemical Reviews*, 107(10):4304-4330, 2007.

[12] Goy, R., Bertini, L., Elleouet, C., Görls, H., Zampella, G., Talarmin, J., De Gioia, L., Schollhammer, P., Apfel, U. P., and Weigand, W. A Sterically Stabilized Fe^{I}–Fe^{I}

Semi-Rotated Conformation of [FeFe] Hydrogenase Subsite Model. *Dalton Transactions*, 44(4):1690-1699, 2015.

[13] Thomas, C. M., Liu, T., Hall, M. B., and Darensbourg, M. Y. Series of Mixed Valent Fe(II)Fe(I) Complexes That Model the H_{ox} State of [FeFe] Hydrogenase: Redox Properties, Density-Functional Theory Investigation, and Reactivities with Extrinsic CO. *Inorganic Chemistry*, 47(15):7009-7024, 2008.

[14] (a) Lavallo, V., Canac, Y., Präsang, C., Donnadieu, B., and Bertrand, G. Stable Cyclic (Alkyl)(Amino)Carbenes as Rigid or Flexible, Bulky, Electron-Rich Ligands for Transition-Metal Catalysts: a Quaternary Carbon Atom Makes the Difference. *Angewandte Chemie International Edition*, 44(35):5705-5709, 2005. (b) Lavallo, V., Canac, Y., DeHope, A., Donnadieu, B., and Bertrand, G. A Rigid Cyclic (Alkyl)(Amino)Carbene Ligand Leads to Isolation of Low-Coordinate Transition-Metal Complexes. *Angewandte Chemie International Edition*, 44(44):7236-7239, 2005. (c) Soleilhavoup, M. and Bertrand, G. Cyclic(Alkyl)(Amino)Carbenes (CAACs): Stable Carbenes on the Rise. *Accounts of Chemical Research*, 48(2):256-266, 2015. (d) Präsang, C., Donnadieu, B., and Bertrand, G. Stable Planar Six-π-Electron Six-Membered N-Heterocyclic Carbenes with Tunable Electronic Properties. *Journal of the American Chemical Society*, 127(29):10182-10183, 2005. (e) Krahulic, K. E., Enright, G. D., Parvez, M., and Roesler, R. A Stable N-Heterocyclic Carbene with a Diboron Backbone. *Journal of the American Chemical Society*, 127(12), 4142-4143, 2005. (f) Iglesias, M., Beetstra, D. J., Knight, J. C., Ooi, L. L., Stasch, A., Coles, S., Male, L., Hursthouse, M. B., Cavel, K. J., Dervisi, A., and Fallis, I. A. Novel Expanded Ring N-Heterocyclic Carbenes: Free Carbenes, Silver Complexes, and Structures. *Organometallics*, 27(13):3279-3289, 2008.

[15] (a) Becke, A. D. Density-Functional Exchange-Energy Approximation with Correct Asymptotic Behavior. *Physical Review A*, 38(6):3098-3100, 1988. (b) Perdew, J. P. Density-Functional Approximation for the Correlation Energy of the Inhomogeneous Electron Gas. *Physical Review B*, 33(12):8822, 1986.

[16] (a) Frisch, M. J., Trucks, G. W., Schlegel, H. B., Scuseria, G. E., Robb, M. A., Cheeseman, J. R., Montgomery, Jr., J. A., Vreven, T., Kudin, K. N., Burant, J. C., Millam, J. M., Iyengar, S. S., Tomasi, J., Barone, V., Mennucci, B., Cossi, M., Scalmani,

G., Rega, N., Petersson, G. A., Nakatsuji, H., Hada, M., Ehara, M., Toyota, K., Fukuda, R., Hasegawa, J., Ishida, M., Nakajima, T., Honda, Y., Kitao, O., Nakai, H., Klene, M., Li, X., Knox, J. E., Hratchian, H. P., Cross, J. B., Bakken, V., Adamo, C., Jaramillo, J., Gomperts, R., Stratmann, R. E., Yazyev, O., Austin, A. J., Cammi, R., Pomelli, C., Ochterski, J. W., Ayala, P. Y., Morokuma, K., Voth, G. A., Salvador, P., Dannenberg, J. J., Zakrzewski, V. G., Dapprich, S., Daniels, A. D., Strain, M. C., Farkas, O., Malick, D. K., Rabuck, A. D., Raghavachari, K., Foresman, J. B., Ortiz, J. V., Cui, Q., Baboul, A. G., Clifford, S., Cioslowski, J., Stefanov, B. B., Liu, G., Liashenko, A., Piskorz, P., Komaromi, I., Martin, R. L., Fox, D. J., Keith, T., Al-Laham, M. A., Peng, C. Y., Nanayakkara, A., Challacombe, M., Gill, P. M. W., Johnson, B., Chen, W., Wong, M. W., Gonzalez, C., and Pople, J. A. *Gaussian 03*, Revision D.02; Gaussian, Inc.: Pittsburgh, PA, 2003. (b) Frisch, M. J., Trucks, G. W., Schlegel, H. B., Scuseria, G. E., Robb, M. A., Cheeseman, J. R., Montgomery, Jr., J. A., Vreven, T., Kudin, K. N., Burant, J. C., Millam, J. M., Iyengar, S. S., Tomasi, J., Barone, V., Mennucci, B., Cossi, M., Scalmani, G., Rega, N., Petersson, G. A., Nakatsuji, H., Hada, M., Ehara, M., Toyota, K., Fukuda, R., Hasegawa, J., Ishida, M., Nakajima, T., Honda, Y., Kitao, O., Nakai, H., Klene, M., Li, X., Knox, J. E., Hratchian, H. P., Cross, J. B., Bakken, V., Adamo, C., Jaramillo, J., Gomperts, R., Stratmann, R. E., Yazyev, O., Austin, A. J., Cammi, R., Pomelli, C., Ochterski, J. W., Ayala, P. Y., Morokuma, K., Voth, G. A., Salvador, P., Dannenberg, J. J., Zakrzewski, V. G., Dapprich, S., Daniels, A. D., Strain, M. C., Farkas, O., Malick, D. K., Rabuck, A. D., Raghavachari, K., Foresman, J. B., Ortiz, J. V., Cui, Q., Baboul, A. G., Clifford, S., Cioslowski, J., Stefanov, B. B., Liu, G., Liashenko, A., Piskorz, P., Komaromi, I., Martin, R. L., Fox, D. J., Keith, T., Al-Laham, M. A., Peng, C. Y., Nanayakkara, A., Challacombe, M., Gill, P. M. W., Johnson, B., Chen, W., Wong, M. W., Gonzalez, C., and Pople, J. A. *Gaussian 09*, Revision D.01, Gaussian, Inc., Wallingford CT, 2009.

[17] (a) Greco, C. and De Gioia, L. A Theoretical Study on the Enhancement of Functionally Relevant Electron Transfers in Biomimetic Models of [FeFe]-Hydrogenases. *Inorganic Chemistry*, 50(15):6987-6995, 2011. (b) Filippi, G., Arrigoni, F., Bertini, L., De Gioia, L., and Zampella, G. DFT Dissection of the Reduction Step in H_2 Catalytic Production by [FeFe]-Hydrogenase-Inspired Models: Can the Bridging

Hydride Become More Reactive than the Terminal Isomer?. *Inorganic Chemistry*, 54(19):9529-9542, 2015.

[18] (a) Perdew, J. P., Burke, K., and Ernzerhof, M. Generalized Gradient Approximation Made Simple. *Physical Review Letters*, 77(18):3865, 1996. (b) Perdew, J. P., Burke, K., and Ernzerhof, M. Generalized Gradient Approximation Made Simple. *Physical Review Letters*, 78(7):1396, 1997. (c) Perdew, J. P., Ernzerhof, M., and Burke, K. Rationale for Mixing Exact Exchange with Density Functional Approximations. *The Journal of Chemical Physics*, 105(22):9982-9985, 1996. (d) Ernzerhof, M. and Scuseria, G. E. Assessment of the Perdew–Burke–Ernzerhof Exchange-Correlation Functional. *The Journal of Chemical Physics*, 110(11):5029-5036, 1999.

[19] Zhao, Y. and Truhlar, D. G. The M06 Suite of Density Functionals for Main Group Thermochemistry, Thermochemical Kinetics, Noncovalent Interactions, Excited States, and Transition Elements: Two New Functionals and Systematic Testing of Four M06-Class Functionals and 12 Other Functionals. *Theoretical Chemistry Accounts*, 120(1-3):215-241, 2008.

[20] (a) Weigend, F. Accurate Coulomb-Fitting Basis Sets for H to Rn. *Physical Chemistry Chemical Physics*, 8(9):1057-1065, 2006. (b) Weigend, F. and Ahlrichs, R. Balanced Basis Sets of Split Valence, Triple Zeta Valence and Quadruple Zeta Valence Quality for H to Rn: Design and Assessment of Accuracy. *Physical Chemistry Chemical Physics*, 7(18):3297-3305, 2005.

[21] (a) Cossi, M., Scalmani, G., Rega, N., and Barone, V. New Developments in the Polarizable Continuum Model for Quantum Mechanical and Classical Calculations on Molecules in Solution. *The Journal of Chemical Physics*, 117(1):43-54, 2002. (b) Tomasi, J. and Persico, M. Molecular Interactions in Solution: An Overview of Methods Based on Continuous Distributions of the Solvent. *Chemical Reviews*, 94(7):2027-2094, 1994.

[22] Addison, A. W., Rao, T. N., Reedijk, J., Rijn, J. v., and Verschoor, G. C. Synthesis, Structure, and Spectroscopic Properties of Copper(II) Compounds Containing Nitrogen–Sulphur Donor Ligands; the Crystal and Molecular Structure of Aqua[1,7-bis(N-methylbenzimidazol-2′-yl)-2,6-dithiaheptane]copper(II)perchlorate. *Journal of Chemical Society Dalton Transaction*, 7:1349-1356, 1984.

[23] (a) Melaimi, M., Jazzar, R., Soleilhavoup, M. and Bertrand, G. Cyclic (Alkyl)(Amino)Carbenes (CAACs): Recent Developments. *Angewandte Chemie International Edition*, 56(34):10046-10068, 2017 and references therein. (b) Roy, S., Mondal, K. C., and Roesky, H. W. CyclicAlkyl(Amino)Carbene Stabilized Complexes with Low Coordinate Metals of Enduring Nature. *Accounts of Chemical Research*, 49(3):357-369, 2016.